Dynamic model of a grooved thrust bearing: Numerical model and experimental validation

AIMETA 2017
XXIII Conference
The Italian Association of Theoretical and Applied Mechanics
Luigi Ascione, Valentino Berardi, Luciano Feo, Fernando Fraternali and Antonio Michele Tralli (eds.)
Salerno, Italy, 4–7 September 2017

DYNAMIC MODEL OF A GROOVED THRUST BEARING: NUMERICAL MODEL AND EXPERIMENTAL VALIDATION

Federico Colombo[1], Luigi Lentini[2,*] , Terenziano Raparelli[3], Andrea Trivella[4] and Vladimir Viktorov[5]

Politecnico di Torino, *Department of Mechanical and Aerospace Engineering*, Turin (Italy).
e-mail: federico.colombo@polito.it [1], luigi.lentini@polito.it [2,*], terenziano.raparelli @polito.it [3],
andrea.trivella@polito.it [4], vladimir.viktorov @polito.it [5],

Keywords: gas bearings, dynamic , grooved, aerostatic bearings, identification

Abstract. *Aerostatic thrust bearings are widely used in applications where high accuracy is requested, e.g., machine tools, measuring instruments, precise positioning systems, manufacturing and medical equipment. Conventional procedures to select or design aerostatic thrust bearings are commonly based on their static characteristics. The prediction of their dynamic behaviour is essential since the dynamic loads affecting this kind of bearings may significantly compromise their performance. This paper presents a dynamic model of a grooved rectangular aerostatic thrust bearing whose results have been experimentally validated on a frequency range from 0 up to 200 Hz, employing a sweep identification test.*

b	Bearing dimension along the x-axis
b_G	Groove length along the x-axis
c	Bearing damping
c_d	Discharge coefficient of supply holes
d_s	Diameter of the bearing supply holes
F	Bearing load capacity
F_a	Amplitude of force oscillations
F_s	Static force
f	Frequency
f_s	Sampling frequency
G	Bearing air consumption
G_{in}	Flow rate provided by the ATB supply holes (Experimental)
G_{th}	Flow rate provided by the ATB supply holes (Theoretical)
h	Bearing air gap height
h_a	Amplitude of air gap height oscillations
h_s	Static air gap height
$H(\Omega)$	Bearing transfer function
K	Static stiffness
k	Dynamic stiffness
L	Bearing dimension along the y-axis
L_G	Groove length along the y-axis
p	Air gap pressure
p_a	Ambient pressure
p_c	Downstream pressure at the ATB holes
p_s	Upstream pressure at the ATB holes
R	
T	Air gap temperature
t	Time
w_h	Flow rate per unit area related to ATB supply holes
X	x-axis of the Cartesian reference frame
Y	y-axis of the Cartesian reference frame
Δx	Length of model elements along the x-direction
Δy	Length of model elements along the x-direction
ΔA	Area of model elements
Ω	Excitation frequency
μ	Air gap viscosity
ρ	Air gap density
φ	Bearing phase lag

Table 1: List of Symbols

ATB	Aerostatic Thrust Bearing
FRF	Frequency Response Function
FT	Fourier Transform

Table 2: List of Acronyms

1 INTRODUCTION

Due to their distinctive features, Aerostatic Thrust Bearings (ATBs) are widely employed in applications where high accuracy is requested, e.g., high speed spindles [1, 2], machine tools [3, 4], measuring instruments [5], precise positioning systems [6, 7], manufacturing and medical equipment [8]. Thanks to their low friction, wear and losses, they make it possible to achieve very smooth and accurate positioning . The performance of conventional ATBs mainly depends on their:

- supply pressure;
- active surface geometry (e.g, conicity, roughness) and
- feeding system (e.g., compound, pocketed or unpocketed restrictors);

Supply pressures typically vary from 4 to 6 absolute bar, but occasionally, pressurised air can be supplied up to 10 absolute bar or higher by using dedicated compressors and bottled gas respectively [9, 10].

The geometrical features of ATB surfaces are an essential element, since it was found that both recess shapes and roughnesses can considerably influence their performance and stability. Plessers and Snoyes [11] discovered the higher static and dynamic performance of gas bearings with a convergent shape gap. Chen and He [12] provided a valuable analysis on the performance of ATB with different recess shapes (rectangular, spherical and non recessed).

Regarding bearing design, selecting the type, geometry, number and shape of restrictors represents a key aspect. Indeed, restrictors, through their inherent pneumatic resistance, make it possible to restore equilibrium conditions after occurences of load variations (*inherent or passive compensation* [13, 14]). Belforte et. al [15, 16] developed a valuable experimental study providing empirical formulas for assessing the discharge coefficients of different types of pneumatic supply restrictors. Using compound restrictors represents a very widespread technical solution aimed at enhancing ATB performance without using active components, such as integrated valves [17], piezo actuators [18, 14] or other active devices [19]. They consist in simple restrictors surrounded by grooves which can have various geometries. Introducing grooves provides higher and more regular pressure distributions, therefore enhancing ATB static performance, i.e, bearing stiffness and carrying capacity. Literature presents both numerical and experimental studies confirming this higher static performance compared to conventional restrictors, especially for low supply pressures [20, 21, 22, 23].

Additionally, it was demonstrated that employing compound restrictors may significantly compromise ATB dynamic performance by increasing the likelihood of instability. For this reason, accurate dynamic characterisations are essential especially for bearings presenting compound restrictors. The main goal of this kind of procedure is the identification of the (dynamic) stiffness and damping capabilities of ATBs. Generally speaking, dynamic characterisations consist

in exciting the investigated bearing and assessing its dynamic features by analysing its response. Excitation to bearings can be provided in many different ways and they can be categorised into two main types, based on their power spectral density (PSD) distributions. There are broadband and narrowband frequency excitations. Broadband excitations are provided by applying impulsive or step force excitations as input to ATBs. Broadband excitations exhibit a near constant and well distributed energy content over a large frequency band. Conversely, narrowband excitations are commonly obtained with the aid of modal exciters (shakers) which make it possible to focus the energy content of the utilised forcing function in a narrow and well defined frequency range. Bearing responses to this excitation are considered in terms of air gap variations. Bearing dynamic characterisations are usually studied through the analysis of their Frequency Response Functions (FRFs) which is the ratio between the output and the input signal related to the investigated system considered in the frequency domain. This paper presents both a numerical and an experimental investigation regarding the static and dynamic performance of an ATB with grooves and compound restrictors. A numerical distributed model is employed for simulating and predicting both static and dynamic performance of this bearing. Static features are assessed through load, stiffness and air consumption curves of the bearing, whereas the dynamic ones are evaluated by employing a sweep identification test over a frequency band ranging from 0 to 200 Hz.

2 THE AEROSTATIC THRUST BEARING MODEL

A distributed parameter model was used to simulate the ATB both in static and dynamic conditions. The model computes the pressure distribution under the ATB by solving the Reynolds' equation for compressible fluids:

$$\frac{\partial}{\partial x}\Big(\frac{\rho h^3}{12\mu}\frac{\partial p}{\partial x}\Big)+\frac{\partial}{\partial y}\Big(\frac{\rho h^3}{12\mu}\frac{\partial p}{\partial y}\Big)+w_h=\frac{\partial(\rho h)}{\partial t} \tag{1}$$

where h is the air gap height, whereas p, μ and ρ are the air pressure, density and viscosity respectively. w_h is the input flow rate (G_{in}) per unit area provided by the supply holes of the bearing.

$$w_h=\frac{G_{in}}{\Delta x\cdot\Delta y} \tag{2}$$

Based on the following assumptions:

- the fluid is under isothermal conditions
- the supply holes according to ISO 6538 [24]

The theoretical flow rate G_{th} through a hole is computed as:

$$G_{th}=\frac{\pi d_s^2}{4}\frac{0.6855}{\sqrt{RT}}p_s\sqrt{1-\Phi^2} \tag{3}$$

where d_s and p_s are the diameter and the upstream pressure of the supply holes respectively. The term Φ expresses the pressure drop between the upstream (P_s) and downstream (P_c) pressures relating nozzles.

$$\Phi=\frac{\frac{P_c}{P_s}-0.528}{1-0.528} \tag{4}$$

In the presence of sonic flows through holes, Φ is equal to zero and the theoretical flow rate is computed as [25]:

$$G_{th} = \frac{\pi d_s^2}{4} \frac{0.6855}{\sqrt{RT}} p_s \tag{5}$$

Theoretical and experimental flow rates are related through the discharge coefficient c_d proposed by Belforte et al. [16].

$$c_d = \frac{G_{in}}{G_{th}} = 0.85 \left(1 - e^{8.2 \frac{h}{d_s}}\right) \left(1 - 0.3 e^{-0.001 Re}\right) \tag{6}$$

where, Re is the Reynolds' number corresponding to the cross section of the supply hole.

$$Re = \frac{4G}{\pi \mu d_s} \tag{7}$$

The load capacity of the pad is obtained by integrating the gauge pressure distribution on the bearing surface:

$$F = \int_A \Big(p - p_a\Big) dA \tag{8}$$

The dynamic stiffness k and damping c of the ATB are computed by imposing periodic air gap variations at different (static) air gap height values h_s

$$h(t) = h_s + h_a cos(\Omega t) \tag{9}$$

where, Ω is the excitation frequency. The related bearing force is finally computed as the sum of a static (F_s) and dynamic (F_a) contributions

$$F(t) = F_s + F_a cos(\Omega t + \varphi) \tag{10}$$

where φ is the phase lag between $F(t)$ and $h(t)$. Hence, dynamic stiffness and damping are computed by Equations 11 and 12.

$$k = \frac{F_a cos(\varphi)}{h_a} \tag{11}$$

$$c = \frac{F_a sin(\varphi)}{h_a} \tag{12}$$

3 EXPERIMENTAL SET-UP

3.1 The Aerostatic Thrust Bearing (ATB)

Figure 1 sketches the geometry of the investigated ATB. It has a rectangular base with b=75 mm and L= 50 mm. This bearing presents four compound restrictors with a diameter d_s=0.155 mm and a rectangular shape groove (b_G= 55 mm and L_G = 30 mm). These restrictors are located in the middle of each side of the rectangular groove.

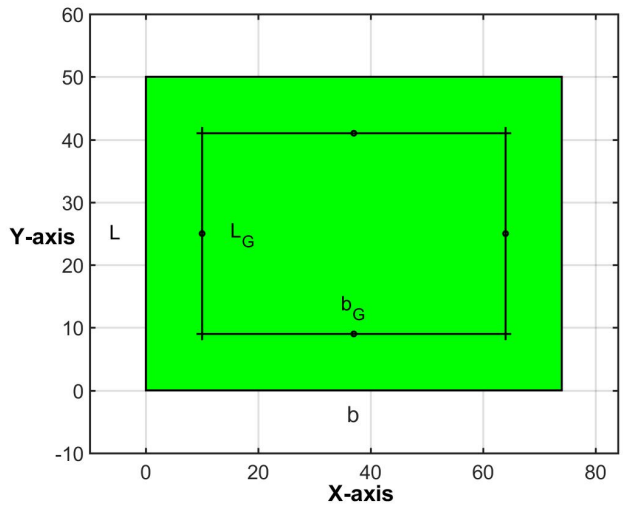

Figure 1: *The ATB geometry.*

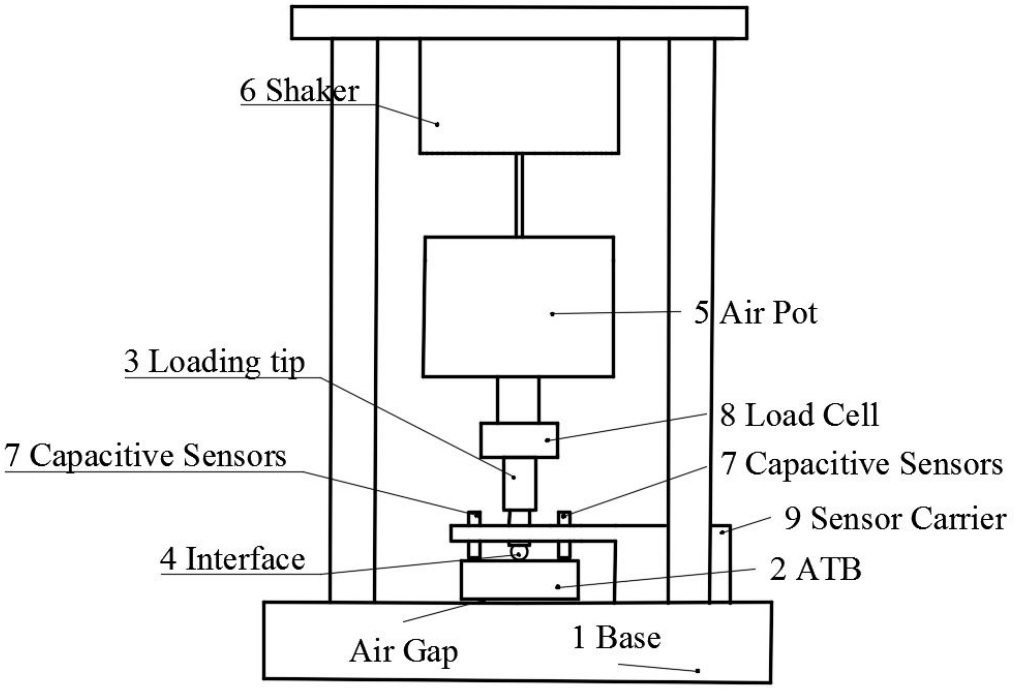

Figure 2: Test rig scheme.

3.2 Test Rig

Figure 2 shows the mechanical structure of the test rig adopted for static and dynamic characterisations of the investigated ATB. The test rig consists of base 1 which supports the investigated ATB 2, which is loaded through small tip 3 and interface 4. Static loads (or pre-loads) are applied on the bearing through air pot 5, whereas dynamic excitations are superimposed to static ones utilising shaker 6. Air gap variations and forces are measured by four capacitive sensors 7 and piezoelectric load cell 8 respectively. Capacitive sensors are placed above the upper surface of the ATB through sensor carrier 9.

4 EXPERIMENTAL PROCEDURES

This section describes the experimental procedures which were adopted to statically and dynamically characterise the investigated ATB. As discussed before, these features depend on the bearing supply pressure and the topology of its bearing surface, i.e, number, dimension and type of the adopted restrictors. Static and dynamic characterisation was performed by employing the test rig described in Section 3.2 where an air pot and a modal exciter respectively provide the static and dynamic loads acting upon the bearing.

4.1 Static

Static characterisations consist in achieving the load, air consumption and stiffness curves of the investigated bearing. These curves respectively plot the load carrying capacity, the air consumption and the stiffness of the bearing as functions of its air gap height, in the presence of a constant supply pressure (P_s= 0.425 MPa). Load and consumption curves were achieved by gradually varying the load applied on the bearing and measuring the correspondent air gap height and air consumption. The stiffness curve was then obtained by the differentiation of the load curve based on the following definition:

$$K = -\frac{dF}{dh} \tag{13}$$

where k is the bearing stiffness, whereas dF and dh are the infinitesimal variation of the external load and the related air gap height variation respectively.

4.2 Dynamic procedure

Assessing the dynamic stiffness and damping capabilities of ATBs is the main goal of dynamic characterisations. Literature describes many different dynamic characterisation procedures which mainly consist in exciting the bearing under test through forcing functions and assessing the dynamic performance by the analysis of its response. Step [18], impulsive [26, 27], sinusoidal [28] and sweep are the most used types of forcing functions. It is worth outlining that this choice is strictly related with the dimension of the investigated frequency range and the signal-to-noise ratio characterising the acquired signals. Bearing response can be analysed using time or frequency domain identification methods [28]. In this study, the dynamic excitations provided were superimposed to static preloads by using a modal exciter. The selected forcing function was a linear sweep with a duration of 80 s, exciting a frequency range from 0 up to 200 Hz. The dynamic features of the bearing was investigated in the presence of a constant supply pressure P_s of 0.425 MPa and at different air gap height h. Figure 3 shows an example of the applied forcing function and the related bearing response expressed in term of air gap height

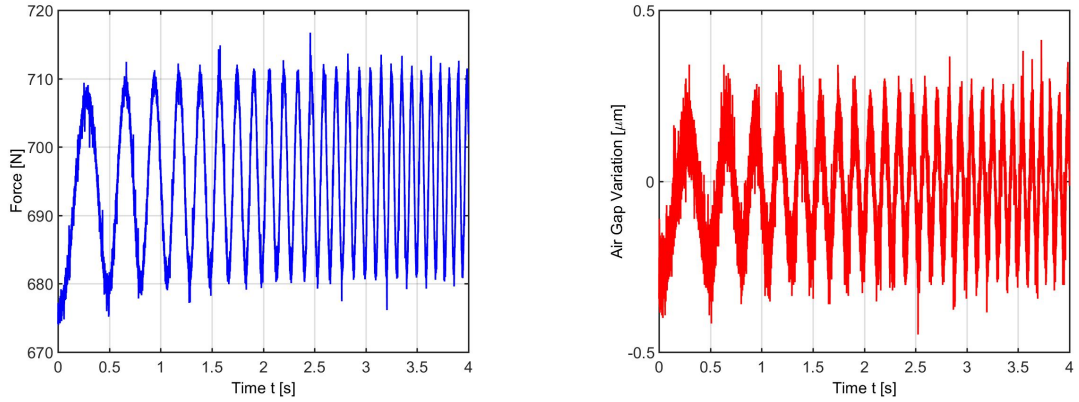

(a) *Force variation versus time (input signal).*

(b) *Air gap height variation versus time (output signal).*

Figure 3: Sweep excitation and bearing response.

variations.
Stiffness and damping coefficients were achieved with the aid of the MATLAB® function *tfestimate* [29]. Given the input and output signals related to the analysed bearing, this function makes it possible to compute the following transfer function $H(\Omega)$

$$H(\Omega) = \frac{F(\Omega)}{h(\Omega)} \tag{14}$$

where, $F(\Omega)$ and $h(\Omega)$ are the transfer functions of the input force and the related air gap variation.

5 RESULTS AND DISCUSSIONS

This section presents experimental results from the static and dynamic bearing characterisation.

5.1 Static

As discussed before, the static performance of the bearing was assessed, in the presence of a constant supply pressure P_s= 0.425 MPa, through a conventional procedure that varied the applied load and simultaneously recorded the air gap height and air consumption (see Section 4.1). Figure 5 compares the experimental and numerical static curves of the bearing. Figures 4(a), 4(b) and 4(c) show respectively the load capacity, the static stiffness and the air consumption of the bearing. Figures 4(a) and 4(b) illustrate the experimental tests on five pads with the same geometry. The experimental results shows some dispersion, due to the tolerance when making the supply holes and the active surfaces of the bearings. Figure 4(b) shows numerical and experimental curves related to the static stiffness of the bearing. Static stiffness curves were achieved by integrating load curves. In this instance, for the sake of clarity, numerical and experimental results are compared by considering only one experimental curve.

5.2 Dynamic

The dynamic characterisation of the bearing was achieved, in the presence of a constant supply pressure P_s= 0.425 MPa, using a numerical model and carrying out experimental tests. Section 2 presents the main equations and assumptions adopted for building the numerical model,

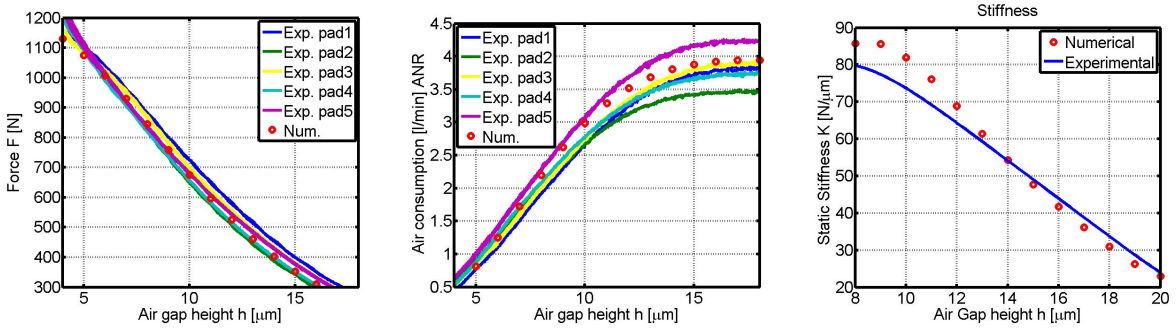

(a) *Load capacity.* (b) *Static stiffness.* (c) *Air Consumption.*

Figure 4: *Static characterisation results: numerical and experimental data.*

whereas Section 4 describes the procedure adopted in performing the dynamic characterisation of the bearing. Figure 5 shows the results obtained from the dynamic characterisation. Figure 5(a) illustrates the dynamic stiffness of the bearing expressed as a function of the excitation frequency f (rad/s) [1] at different air gap heights. The dynamic stiffness exhibits quite similar trends showing peaks with different amplitudes at the same excitation frequencies for all the considered air gap heights. These peaks prove that the bearing undergoes under high oscillations when subjected to forcing functions provided at 110, 165 and 205 Hz. These resonances are also evident from Figure 5(b) which shows trends of the bearing damping over the investigated frequency range. It is clear that the bearing damping drastically decays at frequencies corresponding to these peaks (110, 165 and 205 Hz). A part from this, the bearing exhibits near constant stiffness up to bout 110 Hz for all the considered air gap heights. Figure 6 shows the

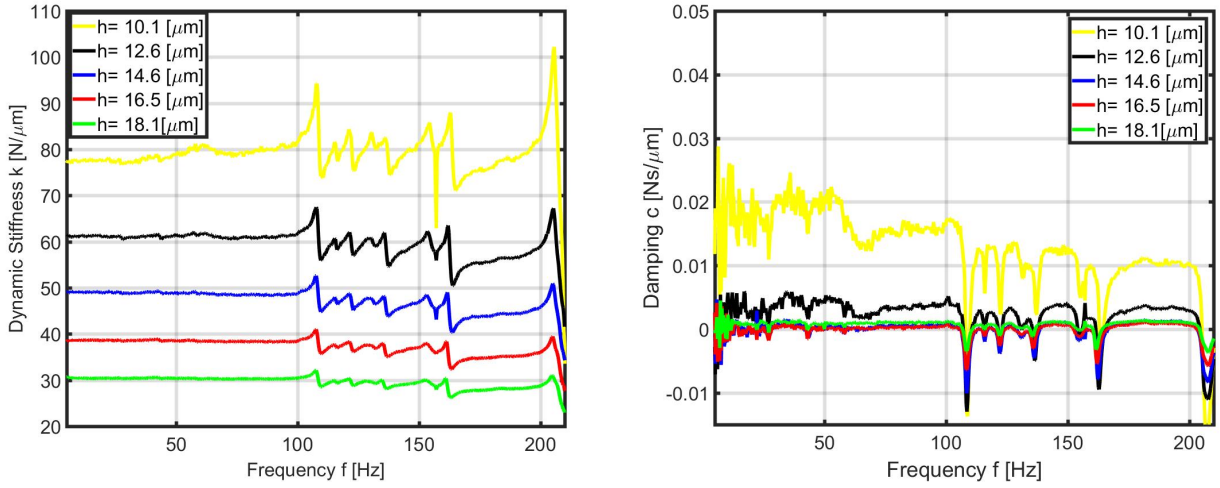

(a) *Dynamic Stiffness.* (b) *Damping.*

Figure 5: *Dynamic characterisation results: numerical and experimental data.*

curves of stiffness and damping obtained both from experimental and numerical tests, considering a constant excitation frequency f=80 Hz. Experimental data were obtained by testing five pads with the same geometry. these results clearly show that dynamic stiffness and damping

[1] $f = \dfrac{\Omega}{2\pi}$

coefficients exhibit non-linear decreasing trends with respect to the bearing air gap height. Furthermore, these results make it possible to better validate the model results and simultaneously statistically assess errors related to the bearing manufacturing. The numerical model acceptably approximates the experimental data.

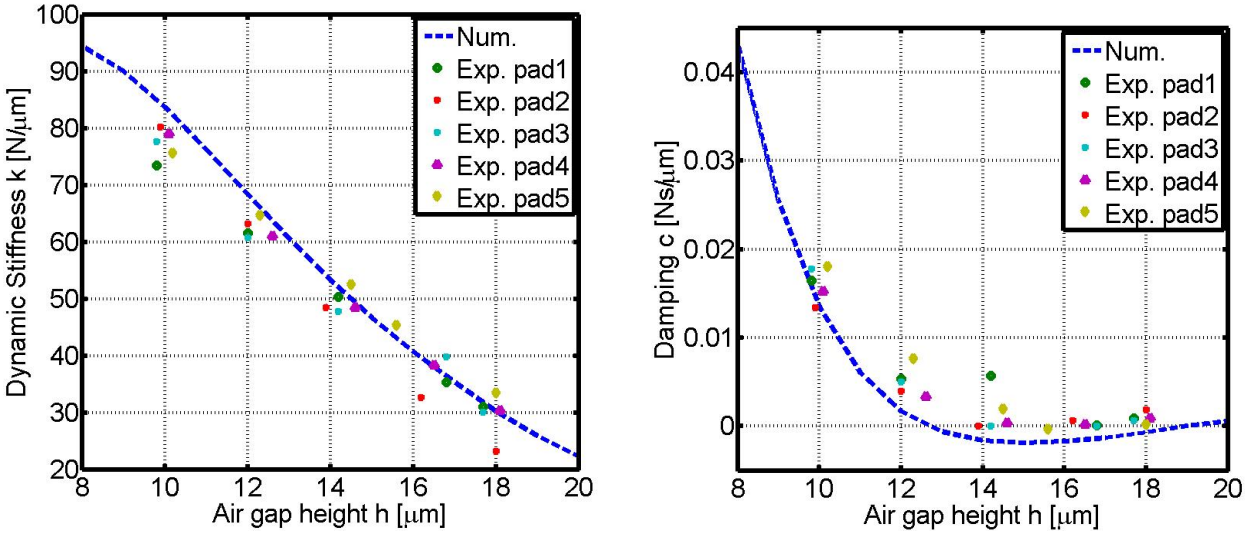

(a) *Dynamic Stiffness.* (b) *Damping.*

Figure 6: *Dynamic characterisation results at 80 Hz: numerical and experimental data.*

6 CONCLUSIONS

Using bearings with grooves (also called compound restrictors) represents a very widespread technical solution to achieve high performance. However, employing compound restrictors may significantly compromise the dynamic performance of the bearing by increasing the likelihood of instability. This paper presents a study of both static and dynamic performance of a grooved rectangular ATB. The bearing characterisation was obtained by using a distributed mathematical model and an experimental sweep identification procedure. The comparison between numerical and experimental results demonstrates the good accuracy of the model. The proposed experimental identification technique makes it possible to detect critical frequencies where the bearing exhibits resonances, therefore proving the value of this methodology. Moreover, the presented numerical and experimental methodology had proven to be a very useful tool for identifying bearing stiffness and damping coefficients.

7 BIBLIOGRAPHY

References

[1] G. Belforte, F. Colombo, T. Raparelli, V. Viktorov, High-speed rotor with air bearings mounted on flexible supports: test bench and experimental results, Journal of Tribology 130 (2) (2008) 21103.

[2] G. Belforte, F. Colombo, T. Raparelli, A. Trivella, V. Viktorov, High-speed electrospindle running on air bearings: design and experimental verification, Meccanica 43 (6) (2008) 591–600. doi:10.1007/s11012-008-9135-5.
URL http://dx.doi.org/10.1007/s11012-008-9135-5

[3] H. L. Wunsch, Air-Bearing Applications to Machine Tools and Measuring Instruments, Journal of Lubrication Technology 90 (4) (1968) 680–686.
URL http://dx.doi.org/10.1115/1.3601699

[4] X. Luo, K. Cheng, D. Webb, F. Wardle, Design of ultraprecision machine tools with applications to manufacture of miniature and micro components, Journal of Materials Processing Technology 167 (2) (2005) 515–528.

[5] W. Gao, Y. Arai, A. Shibuya, S. Kiyono, C. H. Park, Measurement of multi-degree-of-freedom error motions of a precision linear air-bearing stage, Precision engineering 30 (1) (2006) 96–103.

[6] H. Aoyama, I. Watanabe, K. Akutsu, A. Shimokohbe, An Ultra Precision Straight Motion System (1st Report), Journal of the Japan Society for Precision Engineering 54 (3) (1988) 558–563. doi:10.2493/jjspe.54.558.

[7] H. Matsumoto, J. Yamaguchi, H. Aoyama, A. Shimokohbe, An Ultra Precision Straight Motion System (2nd Report), Journal of the Japan Society for Precision Engineering 54 (10) (1988) 1945–1950. doi:10.2493/jjspe.54.1945.
URL http://ci.nii.ac.jp/naid/110001369376/en/

[8] H. Mandroian, Turbine driven air bearing dental handpiece (1964).

[9] J. W. Powell, Design of aerostatic bearings, Machinery's Books for Engineers, Machinery Publishing, 1970.
URL http://books.google.it/books?id=x6EoAQAAMAAJ

[10] W. B. Rowe, Hydrostatic, Aerostatic, and Hybrid Bearing Design, Elsevier, 2012.
URL http://books.google.it/books?id=WX3UMxG86qkC

[11] P. Plessers, R. Snoeys, Dynamic identification of convergent externally pressurized gas-bearing gaps, Journal of tribology 110 (2) (1988) 263–270.

[12] X.-D. Chen, X.-M. He, The effect of the recess shape on performance analysis of the gas-lubricated bearing in optical lithography, Tribology international 39 (11) (2006) 1336–1341.

[13] T. Raparelli, V. Viktorov, F. Colombo, L. Lentini, Aerostatic thrust bearings active compensation: Critical review, Precision Engineering (2015) – doi:http://dx.doi.org/10.1016/j.precisioneng.2015.11.002.
URL http://www.sciencedirect.com/science/article/pii/S0141635915002159

[14] F. Colombo, L. Lentini, T. Raparelli, V. Viktorov, Actively compensated aerostatic thrust bearing: design, modelling and experimental validation, Meccanica (2017) 1–16doi:10.1007/s11012-017-0689-y.
URL http://dx.doi.org/10.1007/s11012-017-0689-y

[15] G. Belforte, T. Raparelli, V. Viktorov, a. Trivella, Discharge coefficients of orifice-type restrictor for aerostatic bearings, Tribology International 40 (3) (2007) 512–521. doi:10.1016/j.triboint.2006.05.003.

[16] G. Belforte, F. Colombo, T. Raparelli, A. Trivella, V. Viktorov, Experimental Analysis of Air Pads with Micro Holes, Tribology Transactions 56 (2) (2013) 169–177. doi:10.1080/10402004.2012.734547.
URL http://dx.doi.org/10.1080/10402004.2012.734547

[17] D. Ghodsiyeh, F. Colombo, T. Raparelli, A. Trivella, V. Viktorov, Diaphragm valve-controlled air thrust bearing, Tribology International 109 (2017) 328–335.

[18] F. Colombo, L. Lentini, T. Raparelli, V. Viktorov, Experimental Identification of an Aerostatic Thrust Bearing, in: Advances in Italian Mechanism Science, Springer, 2017, pp. 441–448.

[19] F. Colombo, D. Maffiodo, T. Raparelli, Active gas thrust bearing with embedded digital valves and backpressure sensors, Tribology Transactions (2016) 1–7.

[20] G. Belforte, F. Colombo, T. Raparelli, A. Trivella, V. Viktorov, Performance of externally pressurized grooved thrust bearings, Tribology letters 37 (3) (2010) 553–562.

[21] G. Belforte, F. Colombo, T. Raparelli, A. Trivella, V. Viktorov, Study of a gas thrust bearing with supply grooves, in: Proceedings of the JFPS International Symposium on Fluid Power, Vol. 2008, 2008, pp. 515–520.

[22] S. Yoshimoto, J. Tamura, T. Nakamura, Dynamic tilt characteristics of aerostatic rectangular double-pad thrust bearings with compound restrictors, Tribology International 32 (12) (1999) 731–738. doi:10.1016/S0301-679X(00)00004-9.

[23] T. Nakamura, S. Yoshimoto, Static tilt characteristics of aerostatic rectangular double-pad thrust bearings with compound restrictors, Tribology international 29 (2) (1996) 145–152.

[24] P. F. P.-C. U. Compressible, Fluids-Determination of Flow-rate Characteristics, ISO 6358 (1989) 1989.

[25] G. Belforte, T. Raparelli, V. Viktorov, Modeling and identification of gas journal bearings: self-acting gas bearing results, TRANSACTIONS-AMERICAN SOCIETY OF MECHANICAL ENGINEERS JOURNAL OF TRIBOLOGY 124 (4) (2002) 716–724.

[26] P. Matta, M. Arghir, O. Bonneau, Experimental Analysis of Cylindrical Air-Bearing Dynamic Coefficients, Tribology Transactions 53 (3) (2010) 329–339. doi:10.1080/10402000903283318.

[27] P. Matta, M. Arghir, Identification method for rotordynamic coefficients of cylindrical air bearing using an impact hammer, Proceedings of the Institution of Mechanical Engineers, Part J: Journal of Engineering Tribology 226 (3) (2012) 199–212. doi:10.1177/1350650111427508.
URL http://dx.doi.org/10.1177/1350650111427508

[28] L. Lentini, Design, Test and Identification of an Active Aerostatic Thrust Bearing with a Compliant Mechanism and Piezo Actuator, Ph.D. thesis, Politecnico di Torino (2017).
URL http://porto.polito.it/2670377/

[29] H. Vold, J. Crowley, G. T. Rocklin, New ways of estimating frequency response functions., Sound & Vibration 18 (11) (1984) 34–38.